



Cruise flight simulation of distributed propulsion and wingtip-mounted propeller aircraft and their validation with in-flight measurement data

M. Schollenberger¹ · M. Firnhaber Beckers¹ · T. Lutz¹ · E. Krämer¹ · D. Bergmann² · J. Denzel² · A. Strohmayer² · O. Pfeifle^{3,4} · W. Fichter³

Received: 16 March 2025 / Revised: 28 May 2025 / Accepted: 11 June 2025 / Published online: 9 July 2025
© The Author(s) 2025

Abstract

The utilization of aerodynamic interactions between propellers and wings through distributed propulsion (DP) and wing tip mounted propellers (WTP) offers a range of advantages for electrically powered aircraft, from improved high-lift behavior to increased aerodynamic efficiency in cruise flight. In the LuFo project VELAN, a DP configuration of the unmanned scaled flight demonstrator e-Genius-Mod is currently being investigated, following the evaluation of a pure WTP variant in the LuFo project ELFLEAN. For both concepts, a numerical analysis with the Reynolds-Averaged Navier–Stokes (RANS)-based flow solver TAU is discussed in this paper and the influence of various parameters is addressed, such as the flight speed and the thrust ratio of the propellers. To ensure a reliable prediction of the cruise flight condition and the aerodynamic effects in the numerical simulations, the CFD methods are validated with experimental data from wind tunnels and in-flight tests. The cruise flight condition in the simulation is achieved by an algorithm for adjusting the propeller thrust to the aircraft drag, resulting in qualitatively and quantitatively accurate results. Both concepts improve the aerodynamic efficiency in cruise flight, which improves as the ratio of WTP thrust to the total thrust increases. In relation to each isolated wing, over 6% increased aerodynamic efficiency can be achieved with the WTP configuration and almost 5% with the DP concept. In absolute values, the optimal WTP aircraft achieves an aerodynamic efficiency of 21.5, which is 3% higher than with the most efficient DP configuration.

Keywords Aerodynamic interactions · Distributed propulsion · Wingtip mounted propeller · Numerical simulation · Actuator disk

List of symbols

AoA Angle of attack
ACD Actuator disk
BET Blade element theory
DP Distributed propulsion
WTP Wingtip mounted propeller
CFD Computational fluid dynamics

RANS Reynolds averaged Navier–Stokes equations
TAU CFD solver of the German Aerospace Center
SARC Spalart–Allmaras turbulence model with rotation correction
SST Menter shear stress transport turbulence model
 v Velocity, m/s
 α Wing angle of attack, °
 β Propeller inclination angle, °
 D Drag, N
 L Lift, N
 r Radius, m
 T Thrust, N
 W Weight, N
 Re Reynolds number, –
 Ma Mach number, –
 b Wing span, m
 c Wing chord, m
 A Wing area, m²

✉ M. Schollenberger
schollenberger@iag.uni-stuttgart.de

¹ Institute of Aerodynamics and Gas Dynamics, University of Stuttgart, Wankelstr. 3, 70563 Stuttgart, Germany

² Institute of Aircraft Design, University of Stuttgart, Pfaffenwaldring 31, 70569 Stuttgart, Germany

³ Institute of Flight Mechanics and Control, University of Stuttgart, Pfaffenwaldring 27, 70569 Stuttgart, Germany

⁴ Present Address: NLR, Amsterdam, The Netherlands

n	Number –
Ω	Rotation speed, rpm
$C_{...}, c_{...}$	Global, local coefficient, –
η	Propulsive efficiency, –
m	Aircraft take off mass, kg
q	Dynamic pressure, kg/(m/s ²)

Indices

Ref	Reference configuration
T	Total
eff	Effective
L, l	Global, local lift
D, d	Global, local drag
exp	Experiment
aver.	Averaged
co	Propeller co-rotating relative to wingtip vortex
contra	Propeller contra-rotating relative to wingtip vortex
off	Propeller not operated

1 Introduction

Propeller-driven aircraft can benefit from the proper utilization of the aerodynamic interaction between the propellers and the wing. The high-lift potential of an aircraft can be strongly increased, due to increased velocity in the propeller slipstream with distributed propulsion (DP) [6, 7]. The cruise flight efficiency instead can be very effectively increased with wingtip mounted propellers (WTP), due to a utilization of the swirl in the propeller slipstream [2, 11, 15]. Recently, a variety of CFD studies on WTP and DP configurations have been conducted either to deepen the understanding of the effects or to evaluate the influence on the required power [2, 6, 7, 11, 15]. However, the simulation methods have not yet been validated with real flight test data to ensure that the expected efficiency benefits can also be achieved under realistic cruising flight conditions. This research gap is being addressed in this study.

The University of Stuttgart is operating an unmanned flight demonstrator, called e-Genius-Mod [1, 9], to test new technologies in a rapid and cost-effective manner. In its basic configuration, it features a single propeller positioned at the empennage, as well as winglets. In the past, the e-Genius-Mod was already used in the ELFLEAN project with WTP in combination with the tail propeller for in-flight measurements [9]. As part of the LuFo project VELAN, the e-Genius-Mod is currently equipped with DP. Thus data of different configurations of the e-Genius-Mod are available to investigate the aerodynamic potential of such configurations. The flight tests with the eGenius-Mod are supplemented by high-fidelity numerical simulations with the second-order finite volume flow solver TAU, developed by the German

Aerospace Center (DLR), employing Reynolds-Averaged Navier–Stokes (RANS) equations [14]. A particular challenge in the subsequent simulation of the flight tests is to ensure thrust-drag and lift-weight equilibrium for the cruise condition examined. An algorithm, previously developed [11] to iteratively adjust the propeller rotational speed as well as the wing angle of attack, is thus utilized in the simulations of the different the e-Genius-Mod configurations to obtain steady-state flight conditions. The propellers are thereby modeled using boundary condition based steady state Actuator Disks (ACD) [10]. Relying on 3D propeller polars as input data, a force calculation via blade element theory (BET) takes into account the influences of the wing on the propeller as well—thus the interaction effects are captured in both ways.

In the work presented the numerical simulations are first validated with windtunnel tests for the propeller input data and subsequently with in-flight measurement data of the e-Genius-Mod in cruise-conditions. For the different configurations of the e-Genius-Mod (DP, WTP) the CFD results in cruise flight are then analyzed and evaluated with respect to the cruise-flight efficiency. Thereby the variation of different operating parameters like the flight velocity and the thrust distribution on the different propellers is evaluated with DP and WTP. Finally, the different configurations of the e-Genius-Mod are compared to each other and conclusions on the design of propeller-driven aircraft are drawn.

2 Configurations

The studies are based on the geometry of the unmanned modular technology test platform e-Genius-Mod, shown in flight in Fig. 1. Developed and manufactured at the University of Stuttgart [1], the e-Genius-Mod is a 1:3 scaled unmanned replica of the manned electric aircraft e-Genius. The modular concept of the unmanned system allows for a



Fig. 1 Test platform e-Genius-Mod in DP config

low-risk and low-cost testing of different systems and components as a technology demonstrator platform. Different configurations for utilizing the interactions have been and are being tested in flight tests at the University of Stuttgart with the e-Genius-Mod, see Fig. 2. The basic configuration has a relatively large wingspan of $b = 5.6$ m and is additionally equipped with winglets. The wing has a chord at the root of $c = 0.317$ m. The basic configuration is powered by a single propeller, positioned at the tip of the vertical stabilizer to minimize drag. In the ELFLEAN project, the e-Genius-Mod was equipped with 2-bladed WTPs to demonstrate the aerodynamic effects and their influence on the overall configuration in flight testing [9]. The configuration includes a main propeller integrated in the empennage and two additional WTPs. A measurement system was developed, which is able to measure the thrust and the power of the WTPs and the main propeller during the flight, see Bergmann [1]. The WTP nacelles, in addition to the motor, also store the measurement system and the battery. In the configuration with WTPs used in ELFLEAN, the e-Genius-Mod has a shortened wingspan of $b = 4.84$ m, including the WTP nacelles, and a total mass of $m = 34.9$ kg. In the LuFo follow-up project VELAN, a DP variant with a total of 8 5-bladed propellers (including WTPs but no main propeller) is being investigated on the e-Genius-Mod. This configuration is currently being used to analyze the high-lift behavior of DP and the possibility of successively reducing the vertical tail due to the use of the DP for active yaw control. The DP configuration has a span of $b = 4.80$ m and the same WTP nacelles. In addition, three further propellers are positioned on each wing side as DP in the outer wing segment with relatively smaller nacelles and inclined $\approx 6^\circ$ downwards. It was found in a CFD-based pre-study with one propeller in front of a wing section, that slightly downward tilted DPs will result in improved high-lift characteristics.

The relevant technical data of the e-Genius-Mod in the WTP and DP configuration are summarized in Tables 1 and 2.

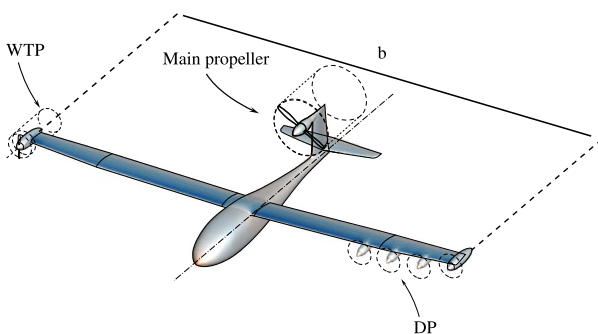


Fig. 2 Numerical setup of the eGenius-Mod

Table 1 Properties of the e-Genius-Mod with WTPs

Aircraft parameter	Value
Wingspan	$b = 4.84$ m
Wing surface area	$A = 1.414$ m ²
Chord length (wing root)	$c = 0.317$ m
WTP radius	$R = 0.127$ m
Take-of mass	$m = 34.9$ kg

2.1 Numerical setup

All numerical simulations in this study were performed using the second-order finite volume flow solver TAU developed by the German Aerospace Center (DLR) [14], which solves Reynolds-Averaged Navier–Stokes (RANS) equations. The influence of the propellers on the wing is modeled by an Actuator Disk (ACD) method [10] based on a boundary condition (BC). A trimming algorithm was used to ensure force equilibrium for steady-state cruise conditions (thrust equals drag and lift equals weight) in the simulation by iteratively adjusting the propeller rotational speed and global angle of attack (AoA) of the aircraft. The algorithm was used before in [11].

The turbulence was either modeled with the Spalart Allmaras turbulence model with rotation correction (SARC) or the two equation Menter shear stress transport model (SST). The simulations are performed fully turbulent neglecting a possible effect of the propeller slipstream on the laminar turbulent transition and an increased viscous drag due to reduced laminar lengths. However, by comparing the first flight test results with first simulations of the airfoil with and without laminar lengths, it was concluded that due to the roughness of the surfaces and the inconstant flight conditions, a profound laminarity is not to be expected. Due to the low Mach number, preconditioning was used in the TAU simulations. The design inflow conditions for the WTP configuration are a Mach number of $M = 0.07$ ($v_\infty = 24$ m/s) and a Reynolds number of $Re = 4.52 \times 10^5$ based on the root chord and $M = 0.074$ ($v_\infty = 25$ m/s) and a Reynolds number of $Re = 5.22 \times 10^5$ for the DP, respectively.

Table 2 Properties of the e-Genius-Mod with DP

Aircraft parameter	Value
Wingspan	$b = 4.80$ m
Wing surface area	$A = 1.414$ m ²
Chord length (wing root)	$c = 0.317$ m
DP radius	$R = 0.13$ m
Take-of mass	$m = 41$ kg

2.1.1 Actuator disk

The TAU ACD generates non-uniform axial and tangential velocity profiles to achieve a physically correct representation of the propeller slipstream influence on the wing. A BET-based force calculation within the ACD model takes into account the influences of the wing on the propeller. Thus, the numerical method is able to capture both the influence of the propeller slipstream on the wing and vice versa of the wing on the propeller forces. The axial and tangential forces are equivalent to those of the propeller (averaged over one propeller revolution) and are introduced via a circular infinitesimally thin disk. The stationary approach of the ACD enables an enormous reduction in computational time compared to fully-resolved propeller simulations. Propeller polars are used as input data, which are generated for each of the three propeller geometries (main propeller, WTP, DP) via a 3D simulation of a single propeller blade operated at different inflow velocities. The exact approach to generate the propeller polar data is described in Schollenberger [12].

2.1.2 Numerical grid

Hybrid grids are used for both configurations, shown in Fig. 3, with structured cells in the BL, the area of the propeller slipstream, and the wing wake. Unstructured cells are utilized in the farfield. The inflow and outflow is realized by a farfield BC at a distance of $100c$. For the DP concept,

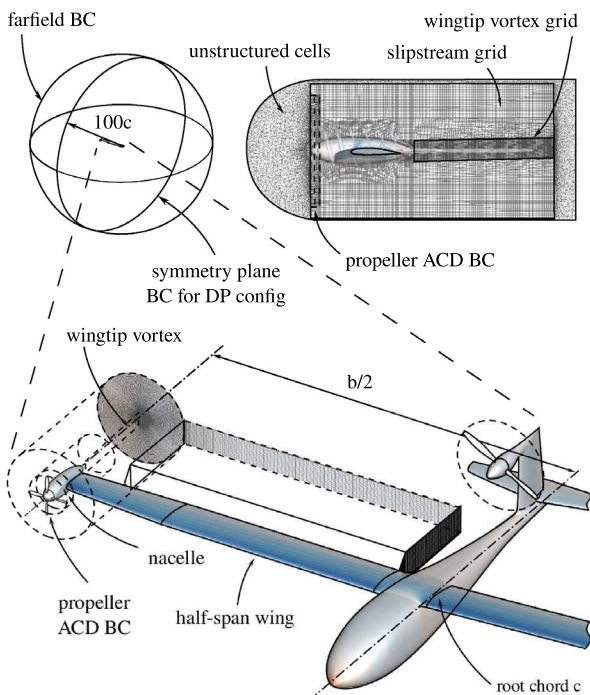


Fig. 3 Numerical grid of the eGenius-Mod half wing

the symmetry is utilized and only a half grid is used to save cells and thus computational time. Due to the central position of the empennage-mounted main propeller in the WTP configuration, a full grid is used here. The wing and fuselage meshes are however otherwise identical.

Prior to the simulations of the aircraft, two grid convergence studies were conducted to investigate the influence of the grid resolution for the isolated wing and an isolated propeller. The grid convergence studies are also shown in [13], where the same wing and propeller resolution was used. Figure 4 shows the deviation of the lift and drag of the wing and the thrust of the propeller to their Richardson extrapolated values. Lift and drag are plotted over the reciprocal value of the total cell number n and the thrust over the product of radial n_r and tangential n_t cell numbers on the propeller disk. An asymptotic decrease can be observed for all coefficients. With a deviation from the extrapolated value of $< 0.5\%$ the resolution of the selected wing grid is considered sufficiently accurate. The deviation of thrust of the selected propeller grid is even lower with $< 0.1\%$.

The wing of the final grid is resolved with 100 points per upper/lower side of the wing in chordwise direction and approximately 250 points in spanwise direction. The wing BL is resolved with 43 cells in normal direction and fulfills $y^+ < 1$ at the first layer. The meshing strategy of the wing, including the BL and the spacings in spanwise direction, follows the guidelines of the AIAA drag prediction workshop [8]. For the propeller grid a cylindrical approach is used. Based on the results of the isolated propeller grid convergence study, the propeller wake area has a mesh resolution corresponding to a cell size of 1.5% relative to the wing root chord c to preserve the slipstream at least until it passes over the wing. In the area of the tip vortex a refinement with a cell size of $0.5\%c$ is used, as found necessary to resolve the wingtip vortex qualitatively well. The fuselage BL is resolved with 30 cells in normal direction also fulfilling the $y^+ < 1$ condition. The final grid for the WTP configuration

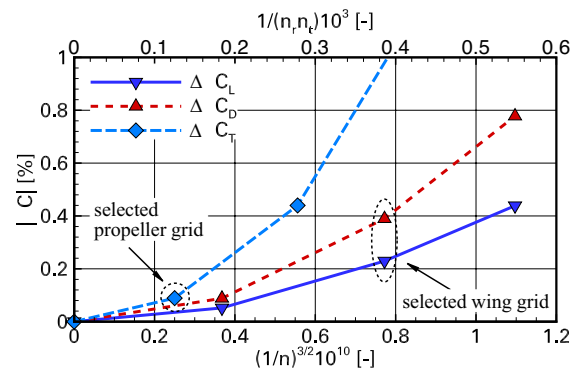


Fig. 4 Grid convergence study

has a total number of points of ≈ 19.5 M and for the DP (half grid) of ≈ 11 M.

2.1.3 Cruise algorithm

To be able to compare the CFD results with flight-test data and different parameter settings (which alter thrust and lift), it is crucial that cruise conditions are reached. A trimming algorithm is used to adjust cruise conditions in the CFD simulation, see Fig. 5. It combines two iteration loops to reach lift and weight ($L = W$) equilibrium by an AoA iteration and thrust and drag ($T = D$) equilibrium by a rotational speed (RPM) iteration. For the AoA iteration, a TAU-internal loop is used which adjusts to a specified global lift coefficient C_L . For the rotational speed iteration, TAU is embedded in an additional external loop where a secant method is used to adjust the thrust to the aircraft drag determined by CFD. Thus, it is basically a zero point search for the function $T - D = 0$. The indirect influence of the AoA iteration and the direct influence of the interactions on the aircraft drag is therefore taken into account in the thrust and drag equilibrium. The calculation procedure is: first, a fully converged TAU calculation is performed with the RPM of the isolated propeller design data. Then, a second TAU calculation is started with a 10% reduced RPM. This allows the secant method to start the thrust iteration loops. In each loop around 1000–1500 iterations are calculated at a constant rotational speed with the TAU-internal AoA iteration before the rotational speed is then varied. In most cases only 2–3 loops are needed to reach a deviation from $T = D$ equilibrium of $< 0.2\%$.

With the cruise algorithm, the vertical and horizontal equilibrium is ensured and the effect of the WTP/DP on the aircraft drag due to the interactions and the lift increase is captured. Instead, the rotational (or longitudinal) equilibrium is not considered when trimming the aircraft and a possible effect of the WTP/DP on the pitching moment and consequently on trim drag is thus neglected. In a high-lift case, i.e., at take-off, the lift due to the DP could require a

different elevator deflection resulting in a severe trim drag. However, since a cruise case is considered here, where the lift increase is rather small, the increase of the pitching moment is expected to be negligible.

3 Validation

To ensure a physically correct representation of the cruise flight simulations, two validation cases are considered. First, the results of the propeller polars as input data of the ACD method are compared with those of wind tunnel tests with the isolated WTP. Subsequently, a comparison of the flight test and CFD data is performed to verify the accuracy of the cruise algorithm and the numerical setup.

3.1 Propeller simulation

In preparation for the flight tests with the WTP configuration in the ELFLEAN project, thrust measurements were carried out on the medium wind tunnel of the IAG, including wake measurements, which are used here for validation of the numerical methods. The geometry of the Aeronaut 10x7 modeling propeller which served as a WTP [9] has a radius of $R = 0.127$ m and the rotational speed of the experiments is 10,000 RPM at the design inflow velocity of 25 m/s. The propeller blade polars were generated using a 3D single propeller blade simulations for a range of advance ratios between $v = (15\text{--}45$ m/s). The measurement setup is shown in Fig. 6. The medium wind tunnel of the IAG is of closed design with an open test section.

In Fig. 7, the influence of the rotational speed on the accuracy of the thrust coefficients and in Fig. 8 the influence of a changing inflow velocity on the accuracy of the wake values in the propeller slipstream are shown. With the single blade simulation a deviation of $\Delta C_T < 1\%$ is achieved for the design point of the propeller grid. The deviations increase with a variation in speed, e.g., for a change in speed of $\Delta|\text{RPM}| < \pm 10\%$ the thrust deviation remains below $\Delta C_T < 5\%$, for a deviation of $\Delta|\text{RPM}| < \pm 20\%$ at least below $\Delta C_T < 10\%$. The discrepancy between numerical and experimental results is in the same range as in similar validations known from literature, see Ciliberti and Nicolosi [4]. The propeller polars are therefore able to capture slightly changed inflow conditions. It can thus be expected that effects due to propeller-wing interactions are captured with sufficient accuracy with a BET-based ACD. Figure 8 shows the dynamic pressure in the slipstream over the propeller radius for different inflow velocities, namely $v = 23, 25,$ and 27 m/s. The procedure for calculating the propeller polars is associated with certain inaccuracies. On the one hand, specifically in this case, the exact propeller geometry was not available, which is why a 3D scan of a propeller

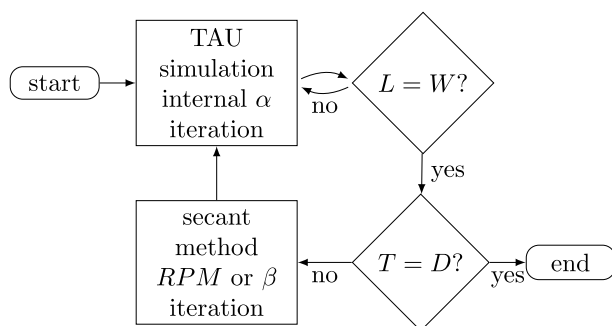


Fig. 5 Flowchart of the cruise algorithm

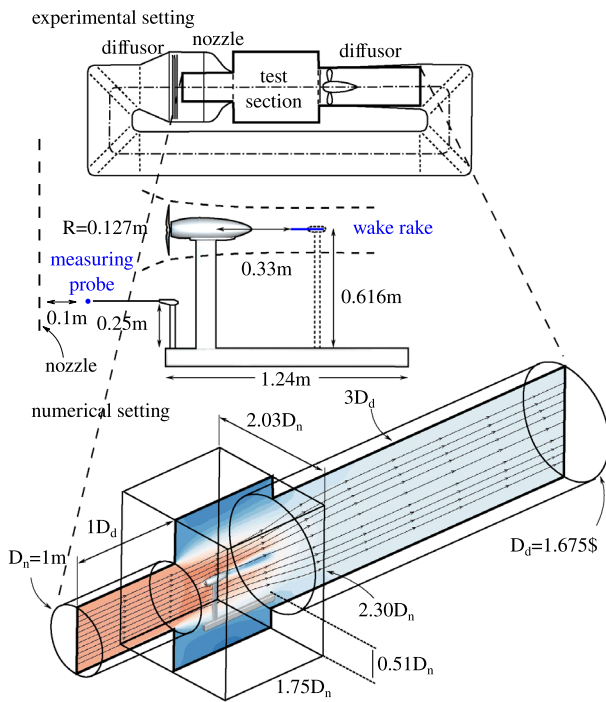


Fig. 6 Experimental and numerical setup of the ELFLEAN propeller in the IAG medium wind tunnel

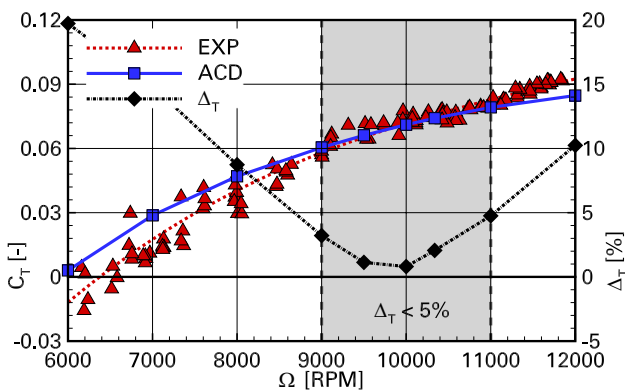


Fig. 7 Global thrust over the rotational speed

blade was carried out. A CAD geometry was then created from the point data and the airfoils were smoothed, which resulted in certain deviations in the airfoil geometry and installation angles. On the other hand, in general, the 3D polar generation method also results in certain inaccuracies due to the grid generation, the local angle of attack determination using a reduced axial velocity method (RAV) and the extrapolation of the local coefficients from the CFD solution, see [12]. To compensate for the simplifications and inaccuracies of the propeller polars, a correction of the propeller blade pitch angle was carried out for the WTP to exactly match the propeller thrust at an inflow velocity of

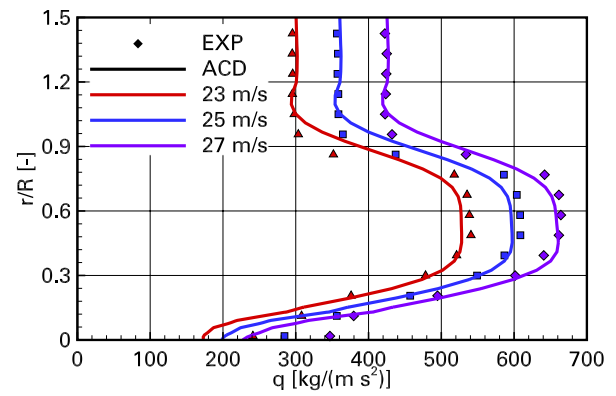


Fig. 8 Local dynamic pressure distribution in radial direction at different inflow velocities

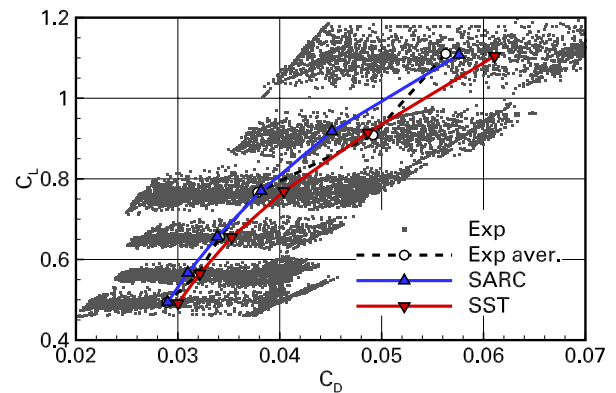


Fig. 9 $C_L(C_D)$ polar with WTP off

25 m/s. The pitch was thereby adjusted by approx. 1° . The resulting calibrated propeller pitch was then kept constant to simulate slightly higher/lower inflow velocities 23 and 27 m/s. The validation with the thrust coefficients and local wake distributions shows a very accurate match with a deviation of less than 1%. The adjustment of the propeller pitch at 25 m/s therefore appears to be justified, as it enables accurate reproduction overall, even at other polar points. The propeller polars as input data for the ACD simulations can therefore be considered valid. Using the same approach, propeller polars were also generated with the scanned geometries of the main propeller and the DP propeller.

3.2 Flight test simulation

Figure 9 and 10 shows the results of the flight tests and their subsequent CFD simulation with the e-Genius-Mod in WTP configuration with the WTP switched off, thus powered only by the main propeller at the tail. The CFD results with two different turbulence models and the experimental data from the flight tests are shown in cruise flight condition. The cruise flight was performed at different flight speeds

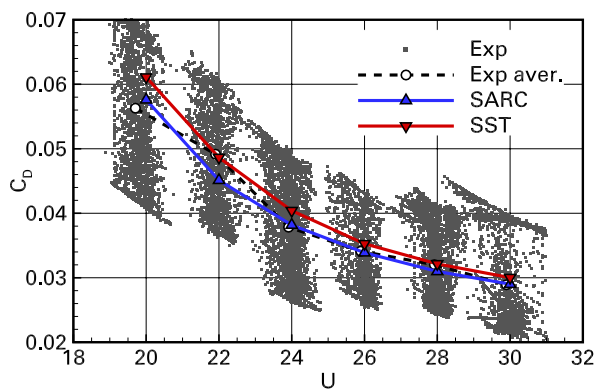


Fig. 10 $C_D(\alpha)$ polar with WTP off

between 20 and 30 m/s. The simulation results are obtained using the cruise algorithm. For the experimental data, both the complete recorded data of a flight and the arithmetically averaged value are shown for each flight speed.

Both turbulence models reflect the averaged C_L/C_D polar curve qualitatively and quantitatively well—lift and drag are therefore captured in the simulation, the steady cruise condition with the algorithm can therefore be considered to be working. The drag is somewhat higher with the SST model than with the SARC. A possible reason could be that the separations are predicted slightly earlier. The experimental averaged values are closer to the SARC result except for 22 m/s and 28 m/s. The assumption that there are no major laminar lengths on the airfoils due to surface quality and inconstant inflow therefore appears to be correct, and the fully turbulent calculation is therefore justified, otherwise a higher deviation should be present. Since the SARC model better resolves the wingtip vortex due to the rotation correction, all further simulations were carried out with the SARC model.

After the comparison with wind tunnel and flight test data, both the input and the output data of the numerical simulations of the propeller-driven configurations can be considered reliable. In the following, it is therefore assumed that physically correct results can also be achieved using the same methods for the WTP and DP configuration and other thrust settings and propeller geometries.

4 Results and discussion

In the following section, the simulation results of the two configurations (WTP and DP) are described and compared with each other in cruise flight. Subsequently, the influence of the ratio of WTP thrust (for DP the outermost propeller) to the total thrust is addressed. All simulation results shown in this section also represent trimmed cruise conditions.

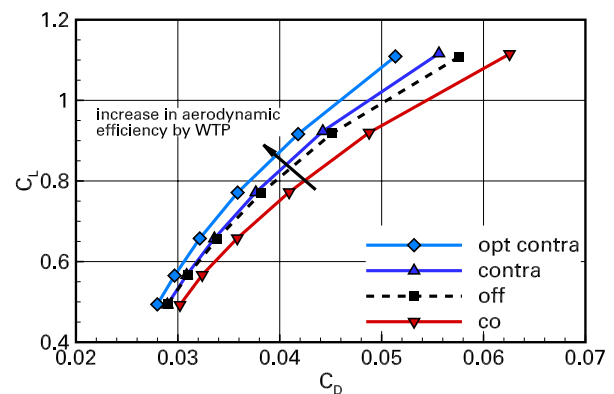


Fig. 11 Lift–drag polar (WTP config.)

4.1 Comparison of WTP and DP

The WTP configuration was flown in a flight test campaign [9] with the two-bladed propeller geometry for the WTPs discussed in the validation section. Figure 11 shows the CFD results of the WTP config. (WTP co- and contra-rotating relative to the direction of rotation of the wingtip vortex). For comparison, the results with the WTP switched off are shown again. The WTP rotational speeds were specified in the simulation according to the flight tests and the thrust of the main propeller was iterated with the algorithm to achieve cruise flight conditions. The ratio between WTP thrust and total thrust is approx. 0.7, varying slightly for the different speeds. A slight improvement in aerodynamic efficiency can be seen with contra-rotating WTP and a decrease with co-rotating WTP relative to the reference. The difference between the co and contra rotating WTP is smaller at higher flight speeds. This result is to be expected, as the wing lift coefficients are correspondingly lower at higher speeds and the local change in lift of the WTP is correspondingly lower too. In addition, the WTP thrust was kept largely constant; due to the higher absolute total drag, the WTP thrust ratio is lower for higher speeds, which has a direct influence on the WTP effects, as will be shown below. The positive effect for the propellers used in the flight test is mainly a consequence of the reduction in AoA due to the local increase in lift.

As shown in detail in [13], the fast rotating two-bladed propellers of small radius are not able to effectively utilize swirl recovery on the wing. Due to the high rotational speed, the swirl in the propeller slipstream is low and only a very small part of the tangential kinetic energy contained therein can be recovered at the wing. Therefore, the positive effect for the propellers used in the flight test is mainly a consequence of the reduction in AoA due to the local increase in lift.

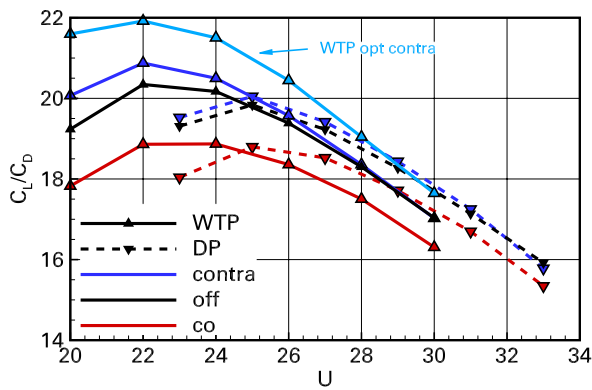


Fig. 12 Aerodynamic efficiency (WTP and DP config.)

contra-rotating WTP optimized for the interactions, a maximal 6% increase in aerodynamic efficiency for the e-Genius Mod was found.

Figure 12 shows the aerodynamic efficiency C_L/C_D of the two configurations over the flight speed U with the propellers on the wing switched off, co-rotating and contra-rotating relative to the wingtip. The results of the WTP configuration are shown with solid lines, those of the DP with dashed lines. Black represents the respective reference configuration (for WTP only with the main propeller in operation, for DP completely without propulsion), blue shows the contra-rotating and red the co-rotating results. The WTP configuration with the propeller used in the flight test has a WTP thrust ratio of approx. 0.7, therefore an almost constant thrust distribution for all three propellers. In the DP configuration with four propellers per half wing, the thrust ratio is also constant with 0.25.

In both cases, the aerodynamic efficiency increases slightly with a counter-rotation while it decreases significantly with a co-rotation. The WTP configuration is found to be generally more efficient than the DP configuration in cruise flight. The optimum of the WTP configuration is at a lower speed than the DP configuration, as the wing load is higher due to the higher weight of the DP configuration with almost the same wing and thus, a higher AoA is required for the same flight speed. For the DP configuration whose intended benefit is the improvement of the high lift potential, which is not addressed in this work, the direction of rotation of the propellers in cruise flight is nevertheless still of considerable importance. The outboard positioned DP also has a slightly positive effect on the aerodynamic efficiency with a contra-rotation relative to the wingtip vortex.

4.2 WTP thrust ratio variation

Since the most outboard positioned propeller (WTP) was identified as the most important propellers for the increase in cruise efficiency, a variation of the WTP thrust ratio was

performed for the WTP and DP configuration. As explained above, the WTPs used in the flight test were not suitable, therefore the optimized propeller was used for the thrust ratio study with WTP-configuration. The thrust ratio was successively increased between 0 (no WTP) and 1 (no other propellers) at constant flight speed $v = 24$ m/s (WTP config.) and $v = 25$ m/s (DP config.), see Fig. 13.

As is to be expected, the aerodynamic efficiency increases with increasing thrust ratio of the WTP and a max. increase of 6% at $T_{WTP}/T = 1$ can be observed. Since the simulation is based on steady flight conditions, this means that there would be a 6% reduction in the required power assuming an identical propeller propulsive efficiency. The actually achieved propeller efficiency is not considered here, as the thrust reduction of the main propeller means that it is increasingly operated outside its optimum efficiency range and decreases accordingly. In reality, however, a different propeller would be designed for a different desired thrust ratio, so that the efficiency analysis is not comparable. For example, the efficiency for $T_{WTP}/T = 1$ is higher than for $T_{WTP}/T = 0$, as the total propeller disk area is larger for both WTPs, which reduces the axial losses in the propeller jet—the propeller efficiency is primarily a question of the propeller design, which is not the focus here.

The influence of the higher T_{WTP}/T can also be seen in the local spanwise lift and drag distribution, see Fig. 14. With increasing T_{WTP}/T , the local lift in the area covered by the WTP propeller slipstream increases and the drag decreases—swirl recovery is therefore increasingly carried out on the wing. Due to the indirectly achieved AoA reduction, the lift in the inner area of the wing decreases compared to a low T_{WTP}/T , as does the drag. For the case of $T_{WTP}/T = 0.25$, a local change in the WTP area is instead hardly visible. In general, a higher WTP thrust component is advantageous.

Drag due to a non-powered empennage-mounted propeller at $T_{WTP}/T = 1$ was, however, not taken into account in the simulation. Thus, the case $T_{WTP}/T = 1$ corresponds to a

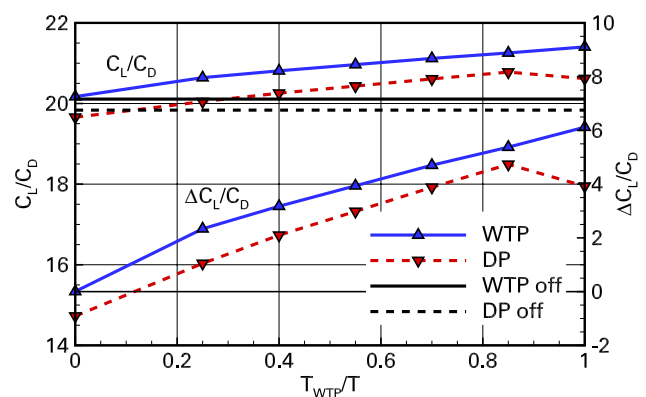


Fig. 13 Aerodynamic efficiency over WTP thrust ratio

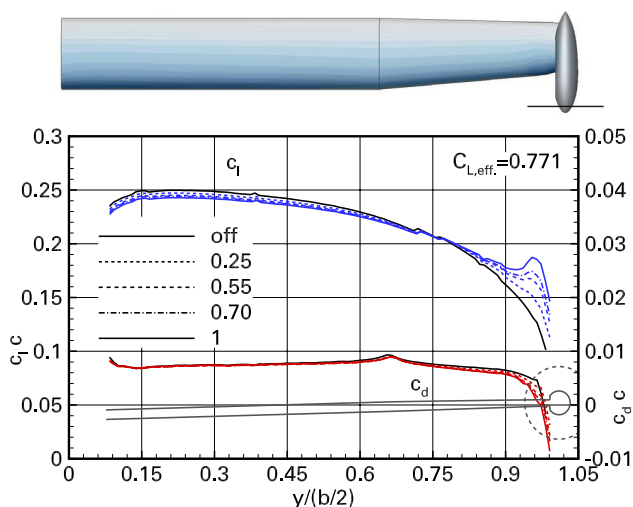


Fig. 14 Local lift distribution of the WTP config

configuration equipped purely with WTP—which is not considered feasible due to the one-engine-out case. In a hypothetical new design of an aircraft intended for WTP use with three propellers in total (two WTPs and one empennage-mounted), it should therefore be clarified what minimum thrust ratio can be achieved for the empennage-mounted propeller in cruise flight with a high propeller efficiency, which in the one-engine-out case still can ensure a safe (albeit inefficient) continued flight.

In principle, the DP configuration also shows an increase in aerodynamic efficiency with increasing shift of the thrust to the WTP (Fig. 13), albeit at a generally lower level. The efficiency increase of the DP configuration is mainly achieved by its WTPs. The results at $T_{WTP}/T = 0$ correspond to a flight with deactivated WTPs—thus only DP driven. The aerodynamic efficiency is even reduced in this case because additional friction on the wing surface due to the DP slipstreams and a non optimal lift distribution overcompensate the swirl recovery effect (Fig. 15). The detrimental effect of pure DP without WTP in cruise was already found by Ciliberti et al. [3]. The opposite case at $T_{WTP}/T = 1$ corresponds to deactivated DPs—thus only WTP driven. A C_L/C_D increase of about 4% can be achieved. However, the maximal increase is at $T_{WTP}/T = 0.85$ with almost 5%—the increasing drag at the second outermost nacelle was identified as the most likely reason why $T_{WTP}/T = 1$ is not optimal here (Fig. 15), as will be discussed below. In absolute values, the optimal WTP aircraft achieves an aerodynamic efficiency of 21.5, which is about 3% higher than with the most efficient DP configuration.

Figures 14 and 15 show the spanwise lift, drag and pressure distribution over the wing surface for both configurations and different thrust ratios according to the trimmed flight conditions in Fig. 13. Even if the propeller load is

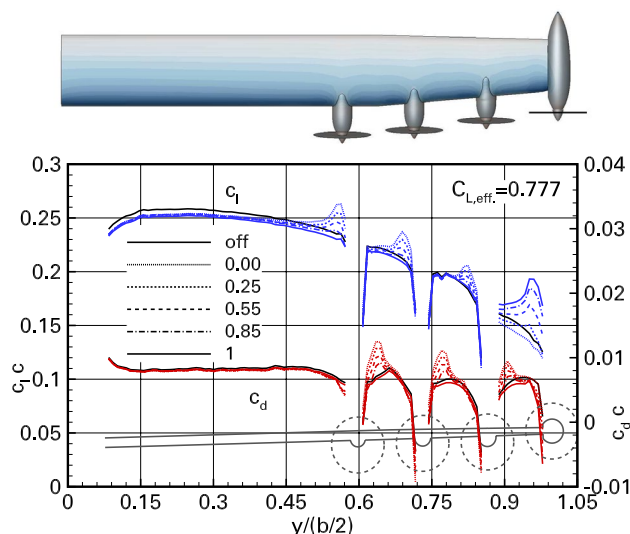


Fig. 15 Local lift distribution of the DP config

small in cruise flight compared to the high-lift case during take-off and landing, the propeller slipstreams still act locally on the wing area covered, which becomes evident in a c_p increase. WTP and DP both increase the lift in the outer area of the wing. As can be seen in the spanwise lift and drag distribution, the WTP effect acts over a larger part of the outer span with increasing thrust. For the DP configuration with $T_{WTP}/T = 1$, the propeller slipstream influence begins to affect the second outer most nacelle, which unfavorably increases the drag. It can be assumed that with a larger distance between the WTP and the second nacelle, this collapse of the aerodynamic efficiency would not occur and a $T_{WTP}/T = 1$ would also be the optimum for the DP configuration.

Also evident in the spanwise distribution is that the deviation of the more inboard propellers decrease with increasing T_{WTP}/T . Since, as shown in Schollenberger [11], the influence of a propeller on the aerodynamic efficiency is more pronounced the further outward it is positioned, the influence of a high thrust ratio in the outer area is positive. However, all DP thrust settings allow a reduction in AoA compared to the reference case (black solid line), which is visible in the reduction of lift in the inner area. What was not investigated is, for example, a linearly increasing thrust distribution towards the WTP, as it can be expected that the second outboard propeller, for example, can perform swirl recovery better than the third, etc. and whether this case would be more efficient overall than maximizing the thrust ratio purely at the WTP.

For aircraft design, it can be concluded that a high thrust component in the WTP is advantageous for both configurations in cruise flight. By comparing the pure WTP configuration with the investigated DP configuration, it can

be assumed that the radius of the WTP propeller and its distance to the DP propellers should be increased for an optimized DP configuration. Another aspect of the DP configuration in aircraft design is the potential reduction in wing area due to the considerable increase in lift in the high-lift case during take-off and landing. No wing area reduction was carried out for the e-Genius-Mod, however the improved climb characteristics and the delayed stall behavior due to the DP are to be investigated in ongoing flight tests inside the VELAN project. In the study presented here, however, only the efficiency increases due to the utilization of the aerodynamic interaction by DP and WTP were quantified under realistic conditions in cruise flight with 5–6%. A possible increase in efficiency due to wing resizing effects compared to a reference aircraft with oversized wings for cruise flight, as shown in Keller [7], is not addressed here. For a new aircraft design, the overall efficiency increase due to DP would depend on aircraft class, flight mission, and the powertrain architecture. With a growth in aircraft weight even an increased energy consumption could be possible with DP [5]. An efficiency increase due to the utilization of the aerodynamic interactions with WTPs in cruise flight can instead be expected.

5 Conclusion

In this study, a WTP configuration and a DP configuration of the unmanned flight demonstrator e-Genius-Mod in cruise flight were examined and compared to flight tests data. The main findings are:

- A precondition for a good prediction in the CFD simulation of propeller-driven aircraft is the quality of the input data for the ACD simulations. In the study, 3D polars were used generated by simulating single propeller blades under varying inflow velocities. A validation with wind tunnel tests shows a close match of the global propeller coefficients with a deviation of less than 5% near the design point. A physically correct representation of the dynamic pressure (hence the axial velocity) in the propeller slipstream was also demonstrated.
- It was shown that by using a cruise algorithm to adjust the propeller thrust and the angle of attack, a steady condition can be achieved which represents realistic cruise flight test conditions. With both the SARC and the Menter-SST model, there is a qualitatively and quantitatively close agreement of the C_L/C_D polar between simulation and flight test.
- The influence of a WTP was studied, including the difference of co- and contra-rotating WTP relative to the wingtip vortex. The difference is a consequence of the possible AoA reduction due to the lift increase in the area

covered by the propeller slipstream with contra-rotating propellers as well as the drag reduction due to the swirl recovery effect and the opposite effects with co-rotating propellers.

- The swirl recovery effect can be increased by using propellers with a higher number of blades and a larger diameter that are optimized for the swirl effects. The DP configuration also shows increased aerodynamic efficiency with contra-rotating propellers and reduced aerodynamic efficiency with co-rotating ones relative to the wingtip vortex, albeit to a smaller extent.
- Furthermore, it could be shown that by increasing the thrust ratio of the WTP relative to the total thrust for both concepts, the positive effects can be increased with over 6% improved aerodynamic efficiency for the pure WTP configuration and approximately 5% for the DP configuration.

The general conclusion for aircraft design is that the thrust share of the WTP should be as high as possible for efficient cruise flight. As a next step for comparing the two general concepts (WTP and DP), it is seen necessary to take into account the reduction in wing area due to the improved high-lift behavior as well as a holistic comparison of the configurations across all phases of the flight mission.

Acknowledgements The authors gratefully acknowledge the Federal Ministry for Economic Affairs and Climate Action (BMWK) for funding this work in the framework of the research project VELAN (FKZ: 20E1919).

Supported by:



on the basis of a decision
by the German Bundestag



Funding Open Access funding enabled and organized by Projekt DEAL.

Data availability Data generated during the study are available from the corresponding author on reasonable request.

Declarations

Conflict of interest The authors have no competing interests to declare that are relevant to the content of this article.

Open Access This article is licensed under a Creative Commons Attribution 4.0 International License, which permits use, sharing, adaptation, distribution and reproduction in any medium or format, as long as you give appropriate credit to the original author(s) and the source,

provide a link to the Creative Commons licence, and indicate if changes were made. The images or other third party material in this article are included in the article's Creative Commons licence, unless indicated otherwise in a credit line to the material. If material is not included in the article's Creative Commons licence and your intended use is not permitted by statutory regulation or exceeds the permitted use, you will need to obtain permission directly from the copyright holder. To view a copy of this licence, visit <http://creativecommons.org/licenses/by/4.0/>.

References

- Bergmann, D.P., Denzel, J., Pfeifle, O., Notter, S., Fichter, W., Strohmayer, A.: In-flight lift and drag estimation of an unmanned propeller-driven aircraft. *Aerospace* (2021). <https://doi.org/10.3390/aerospace8020043>
- Blaesser, N.: Propeller-wing integration on the parallel electric-gas architecture with synergistic utilization scheme (PEGASUS) aircraft (2019). <https://doi.org/10.2514/6.2019-1809>
- Ciliberti, D., Della Vecchia, P., Orticalco, V., Nicolosi, F.: Aeropropulsive interactions between UAV wing and distributed propellers due to their relative position. *Drones* (2023). <https://doi.org/10.3390/drones7010049>
- Ciliberti, D., Nicolosi, F.: Design, analysis, and testing of a scaled propeller for an innovative regional turboprop aircraft. *Aerospace* (2022). <https://doi.org/10.3390/aerospace9050264>
- de Vries, R., Brown, M., Vos, R.: Preliminary sizing method for hybrid-electric distributed-propulsion aircraft. *J. Aircr.* **56**, 1–17 (2019). <https://doi.org/10.2514/1.C035388>. (10)
- Firnhaber Beckers, M., Schollenberger, M., Lutz, T., Bongen, D., Radespiel, R., Florenciano, J., Funes-Sebastian, D.: CFD investigation of high-lift propeller positions for a distributed propulsion system (2022). <https://doi.org/10.2514/6.2022-3217>
- Keller, D.: Towards higher aerodynamic efficiency of propeller-driven aircraft with distributed propulsion. *CEAS Aeronaut. J.* **12**(4), 777–791 (2021). <https://doi.org/10.1007/s13272-021-00535-5>
- Mavriplis, D., Vassberg, J., Tinoco, E., Mani, M., Brodersen, O., Eisfeld, B., Wahls, R., Morrison, J., Zickuhr, T., Levy, D., Murayama, M.: Grid Quality and Resolution Issues from the Drag Prediction Workshop Series. *Journal of Aircraft.* **46**. (2008) <https://doi.org/10.2514/1.39201>
- Pfeifle, O., Notter, S., Fichter, W., Paul Bergmann, D., Denzel, J., Strohmayer, A.: Verifying the effect of wingtip propellers on drag through in-flight measurements. *J. Aircr.* **59**(2), 474–483 (2022). <https://doi.org/10.2514/1.C036490>
- Raichle, A., Melber-Wilkending, S., Himmisch, J.: A new actuator disk model for the tau code and application to a sailplane with a folding engine. In: Tropea, C., Jakirlic, S., Heinemann, H.-J., Henke, R., Hönlinger, H. (eds.) *New Results in Numerical and Experimental Fluid Mechanics VI*. Springer, Berlin (2006). https://doi.org/10.1007/978-3-540-74460-3_7
- Schollenberger, M., Kirsch, B., Lutz, T., Krämer, E., Friedrichs, J.: Aerodynamic interactions between distributed propellers and the wing of an electric commuter aircraft at cruise conditions. *CEAS Aeronaut. J.* (2024). <https://doi.org/10.1007/s13272-023-00706-6>
- Schollenberger, M. and Lutz, T.: Comparison of different methods for the extraction of airfoil characteristics of propeller blades as input for propeller models in cfd, In Dillmann, A., Heller, G., Krämer, E., and Wagner, C., editors, *New Results in Numerical and Experimental Fluid Mechanics XIII*, pages 24–34. Springer International Publishing, (2021), ISBN: 978-3-030-79561-0
- Schollenberger, M., Lutz, T., Bergmann, D.P., Strohmayer, A.: Numerical investigation of the influence of geometric and operational parameters on the aerodynamic interactions of wingtip mounted propellers. In: *AIAA AVIATION 2022 Forum* (2022). <https://doi.org/10.2514/6.2022-3300>
- Schwamborn, D., Gerhold, T., Heinrich, R.: The DLR tau-code: Recent applications in research and industry. In: *ECCOMAS CFD 2006 Conference* (2006). <https://elib.dlr.de/22421/>
- Stokkermans, T.C.A., Nootebos, S., Veldhuis, L.: Analysis and design of a small-scale wingtip-mounted pusher propeller. In: *AIAA Aviation 2019 Forum* (2019). <https://doi.org/10.2514/6.2019-3693>

Publisher's Note Springer Nature remains neutral with regard to jurisdictional claims in published maps and institutional affiliations.